



# Particle size limits for quantitative aerosol analysis using laser-induced breakdown spectroscopy: Temporal considerations<sup>☆</sup>

Michael E. Asgill, David W. Hahn<sup>\*</sup>

Department of Mechanical and Aerospace Engineering, Plasma–Analyte Interaction Working Group, University of Florida, Gainesville, Florida 32611-6300, United States

## ARTICLE INFO

### Article history:

Received 2 January 2009

Accepted 24 July 2009

Available online 5 August 2009

### Keywords:

Laser-induced breakdown spectroscopy

LIBS

Aerosol analysis

Plasma–analyte interactions

## ABSTRACT

The temporal evolution of the Si atomic emission signal produced from individual silica microspheres in an aerosolized air stream was investigated using laser-induced breakdown spectroscopy (LIBS). Specifically, the temporal evolution of Si emission from 2.47 and 4.09- $\mu\text{m}$ -sized particles is evaluated over discrete delay times ranging from 15 to 70  $\mu\text{s}$  following plasma initiation. The analyte signal profile from the microspheres, taken as the silicon atomic emission peak-to-continuum ratio, was observed to follow the same profile of silicon-rich nanoparticles over the range of delay times. The ratio of analyte signals for the 2.47 and 4.09- $\mu\text{m}$  particles was observed to be approximately constant with plasma decay time and less than the expected mass ratio, leading to the conclusion that further vaporization and enhanced analyte response do not continue with increasing delay times for these microsphere sizes. While recent research suggests that the temporal component of analyte response is important for quantitative LIBS analysis, the current study does confirm earlier research demonstrating an upper size limit for quantitative aerosol particle analysis in the diameter range of 2 to 2.5  $\mu\text{m}$  for silica microspheres.

© 2009 Elsevier B.V. All rights reserved.

## 1. Introduction

Laser-induced breakdown spectroscopy (LIBS) remains an important analytical tool for analysis of many sample systems, including for aerosol analysis [1–6]. With recent increased interest in fine particulate matter (e.g. PM<sub>2.5</sub> and PM<sub>10</sub>), including bioaerosols and ambient air aerosol particles, researchers have focused efforts on the development of LIBS-based monitoring techniques [7–12]. Work by Hahn and co-workers has focused on single-shot conditional analysis to improve the sensitivity of the LIBS-based aerosol analysis by taking advantage of the discrete nature of aerosol particles [13–15]. A fundamental issue regarding quantitative LIBS measurements of aerosol particles concerns the assumption of complete breakdown and vaporization of all analyte species that comprise the aerosol particle of interest. Specifically, what is the upper particle size limit for complete dissociation, vaporization and linear analyte response of an individual particle suspended in a gas stream? In some of the earliest LIBS literature regarding particle analysis, Radziemski et al. explored direct LIBS-based analysis of beryllium aerosols using particles less than 10  $\mu\text{m}$  in diameter [1,16], and noted in the latter study that such a particle size is consistent with complete particle vaporization. Over

the ensuing years, several research papers have cited a 10- $\mu\text{m}$  upper size limit for complete particle vaporization [17–18], some referring to the extensive work of Radziemski et al. [1], and some not citing any particular reference source.

In recent years, however, researchers have taken a more detailed look at the upper particle size limits for quantitative LIBS analysis of aerosol particles. Carranza and Hahn explored the vaporization and analyte response of individual silica microspheres in an aerosolized air stream via LIBS [19]. The upper size limit for complete particle vaporization was found to correspond to a silica particle diameter of 2.1- $\mu\text{m}$  for a laser pulse energy of 320 mJ, as determined by the deviation from a linear mass response of the silicon atomic emission signal for progressively increasing diameters of silica microspheres. In addition, comparison of the measured silica particle sampling rates and those predicted based on Poisson sampling statistics and the overall laser-induced plasma volume suggested that the primary mechanism of particle vaporization is related to direct plasma–particle interactions, as opposed to a laser beam–particle interaction. Their findings were discussed in concert with factors that may influence the vaporization dynamics of individual aerosol particles, and it was considered that the larger particles may not have sufficient plasma residence time to completely vaporize on the time-scale that the emission measurements were recorded, namely 35  $\mu\text{s}$  following plasma initiation. This is in agreement with more recent plasma imaging measurements, which demonstrate that the plasma–particle interaction is limited to a spatial region about the particle; hence local plasma conditions may be affected by the presence of large (i.e. micrometer-sized) particles [20]. A more recent study examined

<sup>☆</sup> This paper was presented at the 5th International Conference on Laser-Induced Breakdown Spectroscopy (LIBS 2008), held in Berlin, Adlershof, Germany, 22–26 September 2008, and is published in the special issue of Spectrochimica Acta Part B, dedicated to that conference.

<sup>\*</sup> Corresponding author.

E-mail address: [dwhahn@ufl.edu](mailto:dwhahn@ufl.edu) (D.W. Hahn).

the complete vaporization of carbon-rich particles (specifically glucose particles and sodium hydrogenocarbonate particles) in a laser-induced plasma, and reported an upper size limit of 5  $\mu\text{m}$  for complete vaporization [21]. A larger limiting size with the carbon-rich particles as compared to the silicon particles (2.1 vs. 5  $\mu\text{m}$ ) most likely reflects the marked difference in melting points and volatility when comparing to the more refractory silicon particles to the more volatile particles of the Vors and Salmon study [21].

In view of these and other findings, additional experimental work and plasma modeling are warranted to further determine the exact processes that govern particle vaporization and the ensuing analyte response. Toward this end, Diwakar et al. recently examined the changes in sodium or magnesium LIBS analyte emission response from particle-derived sources with the addition of concomitant mass [22]. Temporally resolved measurements revealed up to a 50% perturbation in analyte emission with the addition of the elements copper, zinc or tungsten, although the enhancement generally diminished by delay times of 60  $\mu\text{s}$ . Additional measurements revealed a general perturbation in localized plasma conditions, as measured by the analyte ion-to-neutral emission ratios, which was attributed to an initial suppression of plasma temperature about the aerosol particles as plasma energy is required to vaporize and ionize the aerosol particle mass resulting from the finite time-scales of particle dissociation, and heat and mass transfer. These measurements provide direct evidence of a thermal matrix effect for aerosol particles, which is attributed primarily to perturbations in the localized plasma properties. Importantly, these perturbations were minimized at longer plasma delay times; suggesting that quantitative LIBS analysis of aerosol particles should be performed with careful attention given to the temporal plasma evolution. In a more recent study by Amodeo et al., a linear LIBS response was reported for sodium and metallic aerosol particles as a function of particle mass in the range from 40 nm up to 1  $\mu\text{m}$  [23]. The Amodeo study stands in contrast to an earlier study by Hohreiter and Hahn, which demonstrated a size-dependency of the analyte response for aerosol particles in the approximately 30 to 100 nm range [24]. However, a critical difference between these two studies was the temporal delay with respect to plasma initiation. Specifically, the Amodeo study used a rather long delay on the order of 50  $\mu\text{s}$ , while the Hohreiter study used a rather short delay of 10  $\mu\text{s}$  with respect to plasma initiation; hence the Amodeo study provides an important additional data point regarding the temporal scales necessary for quantitative analysis. In view of these recent research efforts discussed above regarding the importance of finite heat and mass transfer processes and the resulting perturbations to local plasma conditions, as well as complementary modeling studies [25] and inductively-coupled plasma studies [26], the temporal evolution is a very important parameter with regard to quantifying the analyte response from discrete particles. In view of the recent studies and continued understanding of the plasma-analyte interactions, the present paper reconsiders the upper size limit for complete vaporization of individual silica aerosol particles via the LIBS technique in the context of the ensuing temporal evolution of the analyte response.

## 2. Experimental system and methodology

The LIBS experimental set-up and the aerosol generation system were presented in previous papers [24,27]. Briefly, a 1064-nm Q-switched Nd:YAG laser operating with 300-mJ pulse energy, 10-ns pulse width, and 5-Hz pulse repetition rate was used as the plasma source. The laser pulse energy corresponds to the saturation region with respect to laser pulse energy absorption by the plasma, as reported in an earlier study using the same optical system [28]. For plasma generation, an expanded, 12-mm diameter beam was focused inside the aerosol sample chamber using a 75-mm UV grade plano-convex lens. The plasma emission was collected along the incident beam in a backward direction and separated using a 50-mm elliptical pierced mirror. The

collected plasma emission was launched into an optical fiber bundle, coupled to a spectrometer (2400-groove/mm grating, 0.12-nm optical resolution), and recorded with an intensified charge-coupled device (iCCD) array. Specific detector gates (delay and integration widths) are discussed below.

Aerosols were generated by the nebulization of aqueous solutions of silicon (SPEX ICP-grade silicon standards), and by nebulization of monodisperse silica particle suspensions in deionized water (spherical  $\text{SiO}_2$  particles with monodisperse diameters of either 2.47 or 4.07  $\mu\text{m}$ ). The silica particles were purchased as dry powders (Bangs Labs), and subsequently diluted with ultra-purified deionized water to yield the desired particle concentrations. The particle suspensions were nebulized at a rate of about 0.15 ml/min, and the nebulizer output was subsequently mixed with a gaseous co-flow stream of 42 lpm of purified, dry air. For the case of the monodisperse silica particle suspensions, the particle concentrations in solution were diluted to produce aerosol particle number densities in the range of 50  $\text{cm}^{-3}$  in the LIBS sample chamber. All particle suspensions were subjected to sonication before and periodically throughout all experiments to reduce potential particle agglomeration. For the case of the nebulized aqueous silicon solutions, well-dispersed nanoparticles were produced in the LIBS aerosol sample chamber following droplet desolvation, with a resulting particle size in the range of about 50 to 100 nm and corresponding particle number density in the range of 10<sup>6</sup>  $\text{cm}^{-3}$  [27].

LIBS-based analysis for all experiments used the neutral silicon atomic emission line at 288.16 nm. For all analysis, the LIBS analyte signal was the ratio of the integrated atomic emission line peak area (full-width) to the adjacent continuum base emission intensity, referred to as the peak-to-base (P/B) ratio. The continuum intensity was interpolated using the adjacent, featureless continuum emission intensity on both sides of the silicon emission line. For temporal signal investigation, single-shot spectra were recorded using a series of ICCD gates, including a 15- $\mu\text{s}$  delay and 5- $\mu\text{s}$  integration width with respect to the incident laser pulse (denoted 15/5), and additional gates of 35/5, 50/10 and 70/20- $\mu\text{s}$  for the analysis of the silica microspheres. Additional gates were explored with the nebulized aqueous silicon solutions to further map the silicon temporal analyte response. For the aqueous silicon solutions, ensemble-averaging (minimum of 3000 individual spectra at each known aqueous silicon concentration) was used to quantify the 288.16-nm silicon P/B signal as a function of the temporal gating. These measurements were made at a fixed silicon concentration of 2000  $\mu\text{g}/\text{ml}$  in solution, which yielded a silicon mass concentration of 5.6  $\mu\text{g}/\text{l}$  in the actual LIBS sample chamber. These conditions correspond to a well-dispersed aerosol flow of silicon-rich nanoparticles such that each plasma event samples on the order of 10<sup>3</sup> particles per plasma volume. Such a sampling condition is well-suited for ensemble-averaging.

For the monodisperse silica particle experiments, single-shot conditional analysis was used to identify and analyze individual spectra corresponding to individual silica particles. The conditional data analysis approach was reported previously [9,14–15], and entails the identification of individual LIBS spectra corresponding to the presence of a single, discrete particle based on the targeted analyte atomic emission signal (i.e. silicon peak) exceeding a predetermined threshold value. For the current study, the threshold value for the 288.16-nm silicon emission peak was set to obtain an average of about 5 false hits (i.e. hits recorded for the nebulization of ultra-purified water only) for every 1000 laser shots. After all single-shot spectra that exceeded the threshold were collected, an additional spectral filtering algorithm was then used to screen out false hits and any other anomalous spectra that exceeded the threshold. As noted above, the conditional analysis threshold value was set to allow the detection of a small number of false hits, namely spectra that contain no actual silicon emission, along with very weak or noisy spectra that may correspond to noise events or actual silica particles hits with atypical

spectral response. The presence of a small number of false hits or very weak hits ensures that the single-shot detection threshold is sufficiently low to enable identification of actual analyte hits at signal levels approaching the single-shot noise limit realized for a given spectral location.

The collected spectra were subsequently filtered using the following approach: the filtering algorithm is based on the similarity of the silicon emission line profile for a given single-shot spectrum as compared to the “standard” emission line profile corresponding to the ensemble-average of thousands of individual spectra recorded for the aqueous silicon standard solutions, as described above. Specifically, the silicon line profile of a given single-shot spectrum was compared to the standard line profile using a width of 5 pixels centered about the peak of the actual silicon emission line. Accepted spectra deviated from the template profile by no more than 50% over the left and right pixels, and by no more than 90% over the center pixel. Finally, the lowest 20% of the resulting accepted spectra, as based on the P/B ratio, were rejected for each detector gate. It was observed that the lower 20% of the P/B ratios yielded an identical probability distribution for both the 2.47 and 4.09- $\mu\text{m}$  silica particles, as described below; hence a single threshold was set for each detector gate to remove the bottom 20% using the aggregate cumulative probability distribution of both particle size data sets. Individual inspection of a great number of the rejected 20% of the spectra revealed very noisy spectral data with no clearly discernable silicon emission lines. Overall, this filtering algorithm resulted in the rejection of approximately 40 to 75% of all identified spectrum that exceeded the initial conditional analysis threshold. Most importantly, the spectral rejection rate was consistent for both particle sizes at each respective temporal detection gate.

### 3. Results and discussion

Fig. 1 shows the probability plot of calculated peak-to-base (P/B) ratio of the 288.16-nm silicon atomic emission line for all spectral hits identified for the detector gate of 15/5  $\mu\text{s}$  (width/gate) for the 2.47 and 4.09- $\mu\text{m}$  silica particles. The data correspond to 184 and 175 individual spectra for the 2.47 and 4.09- $\mu\text{m}$  diameters, respectively, that passed the initial spectral filtering algorithm. As noted above, the lower 20% of these identified spectra were then omitted, leaving the

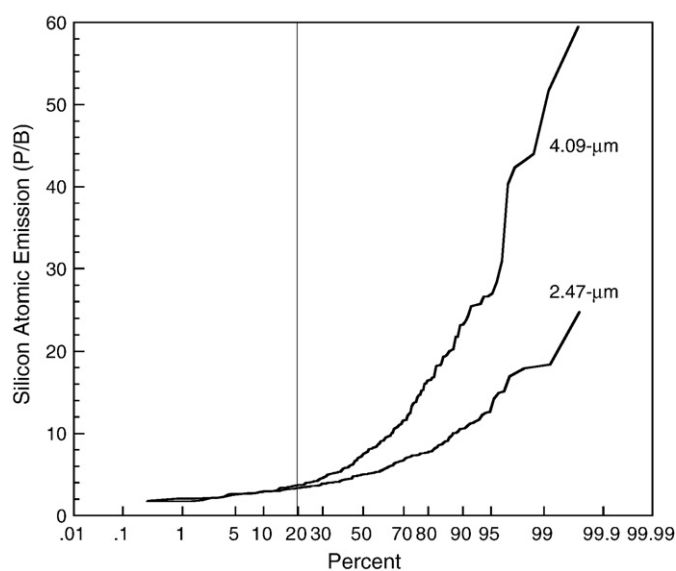


**Fig. 1.** Probability plot of the 288.16-nm silicon emission line (P/B) for the 15/5- $\mu\text{s}$  detector gate corresponding to the 2.47 and 4.09- $\mu\text{m}$  diameter silica microspheres. The vertical line shows the cut-off point (20%) for the final step of the spectral filtering algorithm.

final 138 and 144 spectra for the 2.47 and 4.09- $\mu\text{m}$  diameters, respectively. It is noted that the 20% cut-off was selected for the population of both particle sizes, hence when applied to the individual data sets the exact cut-off percentage varied slightly, ranging from 18 to 25% over all eight data sets. This process was repeated for the detector gates of 35/5, 50/10 and 70/20  $\mu\text{s}$ , resulting in from 105 to 150 final spectra for each detector gate and particle size, noting that for a given gate, the final number of accepted spectra agreed to within 10%. Careful examination of the rejected lower 20% revealed spectra considered well below the single-shot detection limit, with no clear silicon atomic emission peak present. Furthermore, the ensemble-average of the rejected 20% did not reveal a Gaussian spectral profile as observed, for example, with the upper 80% (i.e. accepted) of the spectra or the ensemble-average of the silicon-rich nanoparticles. All data discussed below correspond to the ensemble-average of the silica spectral data that passed the full filtering algorithm for each respective detector gate and particle size.

Representative ensemble-averaged spectra for the 35/5 and 70/20- $\mu\text{s}$  detector gates are presented in Fig. 2 corresponding to both the 2.47 and 4.09- $\mu\text{m}$  diameter silica particles. Several features are noted in Fig. 2. First, for a given detector gate, the two spectra are presented with the identical intensity scale, which reveals an essentially identical continuum emission. This demonstrates that the overall, bulk plasma emission (i.e. integrated over the entire emitting plasma) as represented by the continuum emission, is not altered by the presence of the two different sized silica particles. This is consistent with previous studies, including imaging studies, that conclude that the influence of sample particles are primarily confined to localized regions of the plasma, notably at relatively short delay times, and that the bulk plasma properties are largely unaffected [20,24]. The second feature of Fig. 2 is that for both detection gates, the silicon atomic emission peak corresponding to the 4.09- $\mu\text{m}$  particles is larger than the peak corresponding to the 2.47- $\mu\text{m}$  particles. However, the apparent ratio of the two peak areas appears relatively consistent for the two different detector gates, although this effect is quantified below.

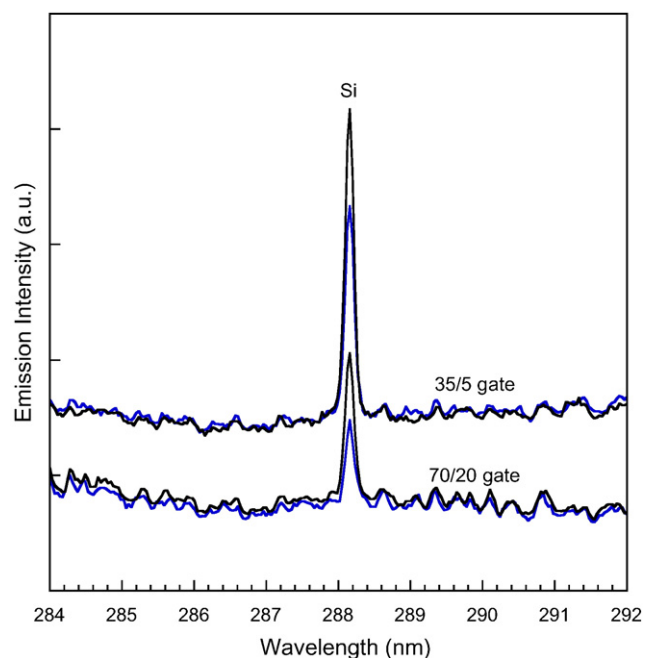


**Fig. 2.** Ensemble-averaged spectra corresponding to two different detector gates (as noted) for the 2.47 and 4.09- $\mu\text{m}$  sized silica microspheres. For each detector gate, the two spectra have the identical intensity scale, with the lower silicon peak corresponding to the 2.47- $\mu\text{m}$  size.

Fig. 3 presents the calculated P/B ratios of the 288.16-nm silicon atomic emission peak as a function of detector gate for the 2.47 and 4.09- $\mu\text{m}$  sized silica microspheres, as well as for the nebulized aqueous silicon solution. It is noted that the aqueous silicon solution results in a very high number density aerosol of silicon-rich nanoparticles, as described above. Therefore, the silicon nanoparticle data correspond to simple ensemble-averages of 3000 laser shots, with no additional spectral filtering algorithm. It is observed that all three P/B data sets reveal the same temporal behavior, with a maximum in the peak-to-base ratio occurring between approximately 30 and 35  $\mu\text{s}$  delay times with respect to plasma initiation. This overall behavior is in agreement with our previous data [19], and corresponds to the optimal point of population of the upper state and subsequent silicon atomic emission as compared to the plasma continuum emission (i.e. recombination and Bremsstrahlung). The specific transition energy ( $6299\text{--}40,992\text{ cm}^{-1}$ ) of the 288.16-nm Si I emission line is consistent with this temporal behavior [29]. The more interesting feature of Fig. 3 is the overall consistency of the temporal data for the two different sized silica microspheres, as quantified below. It is rather difficult to compare the silicon-rich nanoparticle analyte signal (P/B ratio) to the analyte signal of the microspheres, given (1) that the microspheres may not undergo complete vaporization (i.e. beyond the 2.1- $\mu\text{m}$  upper size limit per reference [19]), (2) the variations in the effective sampling volume for the nanoparticles [30], and (3) the uncertainties regarding the size-effects of analyte response [24]. Nonetheless, the experimental ratio of the nanoparticle signal to the 2.47- $\mu\text{m}$  microsphere signal at a delay of 30  $\mu\text{s}$ , based on interpolation of the Fig. 3 data, is in reasonable agreement with the predicted ratio (7 experimental vs. 3.5 predicted) based on the nanoparticle silicon mass concentration (5.9  $\mu\text{g/l}$ ), the estimated representative plasma volume ( $\sim 5\text{ mm}^3$  per references [20] and [30]), and the silicon content of an average 2.47- $\mu\text{m}$  silica particle. The greater experimental ratio is consistent with incomplete vaporization of the silica microspheres, as well as uncertainty in the representative plasma volume, the variability in silica particle analyte response (see Fig. 1), and the potentially reduced signal upon

ensemble-averaging with single-shot analysis of discrete particle events [14,31].

As discussed above, the primary goal of the current study is to examine the temporal behavior of the analyte response of the 2.47 and 4.09- $\mu\text{m}$  silica microspheres, noting that the former size was just beyond the previously reported [19] silica particle size limit for complete vaporization and linear analyte response (2.1  $\mu\text{m}$  diameter). Fig. 4 presents the ratio of the average analyte response of the 4.09- $\mu\text{m}$  particles compared to the response of the 2.47- $\mu\text{m}$  particles as a function of detector gate. The data reveal that the 4.09-to-2.47  $\mu\text{m}$  analyte response ratio is essentially constant with regard to plasma evolution, and significantly less than the ideal ratio of 4.5 (i.e. cube of 4.09/2.47) expected for complete vaporization and subsequent linear silicon mass response. This behavior suggests that these silica particles of diameters 2.47 and 4.09- $\mu\text{m}$  are not completely vaporized in the laser-induced plasmas, thereby confirming our earlier study. Perhaps more importantly, providing additional residence time, even out to 70  $\mu\text{s}$  following breakdown, does not result in additional vaporization and analyte response beyond what is observed through the first 20  $\mu\text{s}$  of plasma evolution.

These results suggest that the plasma-particle vaporization process is controlled by parameters other than simple energy conservation within the plasma, as ample energy exists within the plasma to dissociate a 2.5- $\mu\text{m}$  silica particle, as noted previously [19]. Clearly, process rates must play important roles in the kinetics of particle dissociation, including the diffusion of heat to the dissociating microsphere, and the diffusion of analyte mass throughout the analytical plasma. As noted in recent studies, the scale of both heat and mass transfer are finite and comparable with regard to the relevant time-scales for analytical measurements [20,22,25].

In earlier work, based on both imaging studies and statistical sampling considerations, it was concluded that *plasma-particle* interactions primarily drive the dissociation and vaporization of individual aerosol particles [19,30]. Nonetheless, it is expected that some individual microspheres will be sampled in part directly by the laser beam (i.e. laser beam strikes particle). Initiation of the laser-induced

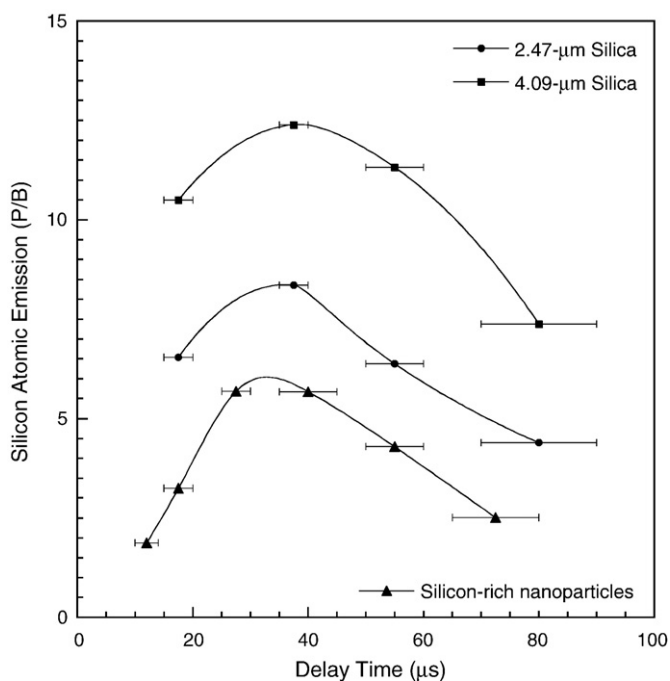


Fig. 3. P/B ratios of the silicon emission line as a function of temporal gating for the 2.47 and 4.09- $\mu\text{m}$  microspheres and for the silicon-rich nanoparticles. The P/B ratios of the silicon-rich nanoparticles have been divided by a factor of 10. The error bars correspond to the detector gate width, with the symbol corresponding to the center of detector gate.

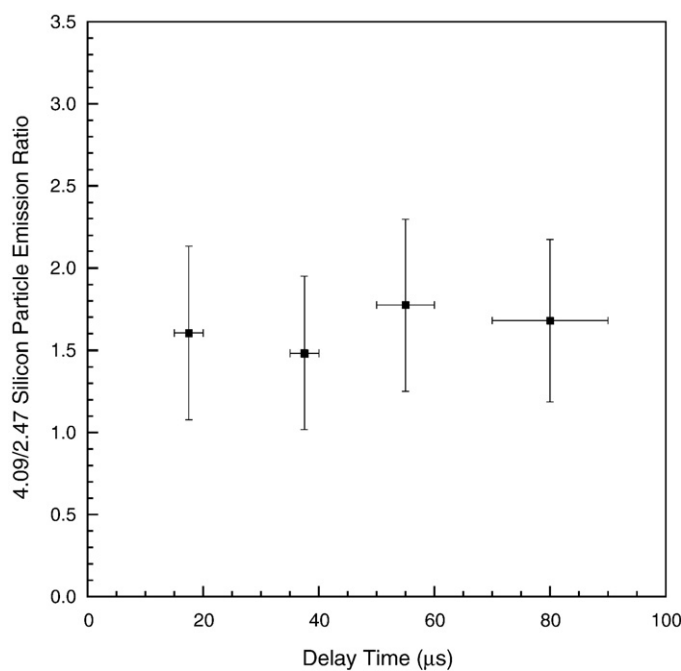


Fig. 4. Ratio of the silicon analyte response of 4.09- $\mu\text{m}$  to the 2.47- $\mu\text{m}$  silica microspheres as a function of plasma evolution time. The x-error bars correspond to the detector gate width, with the symbol corresponding to the center of detector gate. The y-error bars represent the standard deviations of the measurements.

breakdown process by plasma–particle interactions may alter the overall plasma dynamics as well as the resulting analyte response. Such events may partially explain the rather large variation in the distribution of analyte response (i.e. P/B) as observed in Fig. 1. However, direct laser–particle interactions might somewhat expand the regime of linearity by providing additional laser-induced dissociation. While the data in the current study provide no means to differentiate between plasma–particle and laser–particle interactions, it is possible to further analyze the above data sets by considering spectra corresponding only to the largest analyte response. Specifically, for a given particle size and detector gate, the top 10% (by P/B ratio) of the final processed data were separated and ensemble-averaged to examine the resulting analyte response. Fig. 5 shows the results for the 35/5- $\mu$ s gate corresponding to the 2.47- $\mu$ m silica microspheres. The first spectrum corresponds to all previously analyzed particle hits ( $N=122$ ), while the second spectrum corresponds to the top 10%, as measured by P/B ratio, hence to the ensemble-average of 12 spectra.

The results show a clearly enhanced silicon emission peak, as expected by taking the top 10% of the distribution; however, the continuum emission is essentially identical, which is consistent with similar bulk plasma conditions between the two data sets. The top 10% of all data sets were processed and compared as in Fig. 4. Once again, the ratio of the 4.09 to the 2.47- $\mu$ m particle response was found to be essentially constant with plasma evolution, although the average ratio value was slightly higher (2.0 vs. 1.6). It is difficult to assess the significance of the slight enhancement in analyte response ratio for the top 10% of the data. As discussed above, the larger analyte response might represent direct laser–particle interactions, or simply particles closer to the plasma center and therefore subjected to greater plasma temperatures and electron densities. It is noted that the probability of directly sampling a particle with the laser beam is much less than the plasma–particle sampling probability based on Poisson statistics [32]. Either may slightly extend the range of analyte vaporization and response, but clearly, the overall conclusion of non-linearity still holds for these particle sizes.

In summary, the processes that drive aerosol particle vaporization and dissociation are important in controlling the resulting analyte

response. Based on fundamental studies to date, it is clear that these processes are important within the first tens of microseconds following laser-induced breakdown. Furthermore, the kinetics of heat transfer to the sample particle and diffusion of analyte mass away from the particle occur on time-scales that are both finite and comparable. Given these rate-controlled processes in combination with an overall dynamic plasma evolution that is also of a finite time-scale, it is expected that upper size limits will exist for a linear analyte mass response as derived from individual aerosol particles. While the laser-induced plasma as an analytical plasma is a particularly complex and dynamic system, these considerations can also apply to other analytical plasmas, including ICP-MS and LA-ICP-MS. Clearly increased understanding of the overall plasma–analyte interactions will lead to improvements in LIBS as a quantitative analytical technique and may benefit the larger analytical community.

## Acknowledgements

This work was supported in part by the National Science Foundation through grant CHE-0822469, as part of the Plasma–Analyte Interaction Working Group (PAIWG), a collaborative effort of the University of Florida, Federal Institute of Materials Research and Testing (BAM) in Berlin, and the Institute for Analytical Sciences (ISAS) in Dortmund, jointly funded by the NSF and DFG.

## References

- [1] L.J. Radziemski, T.R. Loree, D.A. Cremers, N.M. Hoffman, Time-resolved laser-induced breakdown spectrometry of aerosols, *Anal. Chem.* 55 (1983) 1246–1252.
- [2] W.L. Flower, L.W. Peng, M.P. Bonin, N.B. French, H.A. Johnsen, D.K. Ottesen, R.F. Renzi, L.V. Westbrook, A laser-based technique to continuously monitor metal aerosol emissions, *Fuel Process. Technol.* 39 (1994) 277–284.
- [3] R.E. Neuhauser, U. Panne, R. Niessner, G.A. Petrucci, P. Cavalli, N. Omenetto, On-line and in-situ detection of lead aerosols by plasma-spectroscopy and laser-excited atomic fluorescence spectroscopy, *Anal. Chim. Acta* 346 (1997) 37–48.
- [4] J.P. Singh, F.Y. Yueh, H.S. Zhang, R.L. Cook, Study of laser induced breakdown spectroscopy as a process monitor and control tool for hazardous waste remediation, *Process Control Qual.* 10 (1997) 247–258.
- [5] D.W. Hahn, W.L. Flower, K.R. Hencken, Discrete particle detection and metal emissions monitoring using laser-induced breakdown spectroscopy, *Appl. Spectrosc.* 51 (1997) 1836–1844.
- [6] M.H. Nunez, P. Cavalli, G. Petrucci, N. Omenetto, Analysis of sulfuric acid aerosols by laser-induced breakdown spectroscopy and laser-induced photofragmentation, *Appl. Spectrosc.* 54 (2000) 1805–1816.
- [7] H. Zhang, F.Y. Yueh, J.P. Singh, Laser-induced breakdown spectrometry as a multimetal continuous-emission monitor, *Appl. Opt.* 38 (1999) 1459–1466.
- [8] S.G. Buckley, H.A. Johnsen, K.R. Hencken, D.W. Hahn, Implementation of laser-induced breakdown spectroscopy as a continuous emissions monitor for toxic metals, *Waste Manage.* 20 (2000) 455–462.
- [9] J.E. Carranza, B.T. Fisher, G.D. Yoder, D.W. Hahn, On-line analysis of ambient air particles using laser-induced breakdown spectroscopy, *Spectrochim. Acta Part B* 56 (2001) 851–864.
- [10] J.D. Hybl, G.A. Lithgow, S.G. Buckley, Laser-induced breakdown spectroscopy: detection and classification of biological aerosols, *Appl. Spectrosc.* 57 (2003) 1207–1215.
- [11] P.B. Dixon, D.W. Hahn, On the feasibility of detection and identification of individual bioaerosols using laser-induced breakdown spectroscopy, *Anal. Chem.* 77 (2005) 631–638.
- [12] D. Mukherjee, M.D. Cheng, Quantitative analysis of carbonaceous aerosols using laser-induced breakdown spectroscopy: a study on mass loading induced plasma matrix effects, *J. Anal. At. Spectrom.* 23 (2008) 119–128.
- [13] D.W. Hahn, M.M. Lunden, Detection and analysis of aerosol particles by laser-induced breakdown spectroscopy, *Aerosol Sci. Tech.* 33 (2000) 30–48.
- [14] J.E. Carranza, K. Iida, D.W. Hahn, Conditional data processing for single-shot spectral analysis by use of laser-induced breakdown spectroscopy, *Appl. Opt.* 42 (2003) 6022–6028.
- [15] B. Hettinger, V. Hohreiter, M. Swingle, D.W. Hahn, Laser-induced breakdown spectroscopy for ambient air particulate monitoring: correlation of total and speciated aerosol counts, *Appl. Spectrosc.* 60 (2006) 237–245.
- [16] M. Essien, L.J. Radziemski, J. Sneddon, Detection of cadmium, lead and zinc in aerosols by laser-induced breakdown spectrometry, *J. Anal. At. Spectrom.* 3 (1988) 985–988.
- [17] D.K. Ottesen, J.C.F. Wang, L.J. Radziemski, Real-time laser spark spectroscopy of particulates in combustion environments, *Appl. Spectrosc.* 43 (1989) 967–976.
- [18] S. Yalcin, D.R. Crosley, G.P. Smith, G.W. Faris, Spectroscopic characterization of laser-produced plasmas for in situ toxic metal monitoring, *Hazard. Waste Hazard. Mater.* 13 (1996) 51–61.

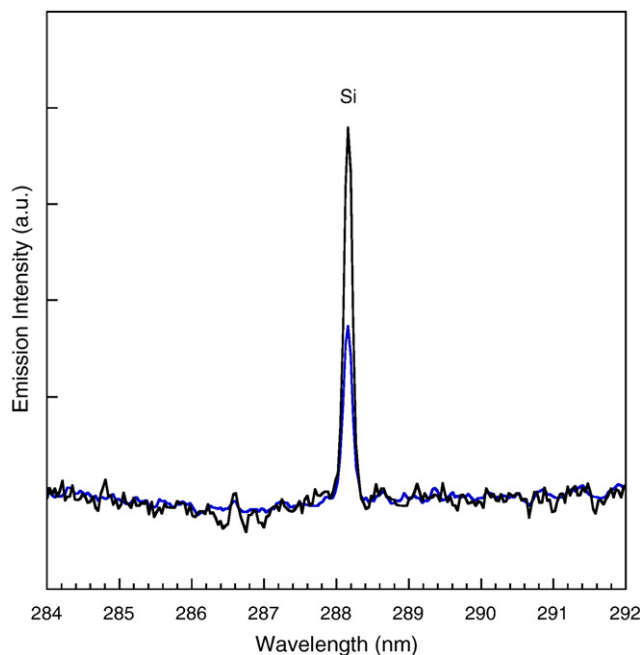


Fig. 5. Ensemble-averaged spectra corresponding to the full data set and the top 10% for the 2.47- $\mu$ m sized silica microspheres and the 35/5- $\mu$ s gate. The lower silicon peak corresponds to full data set. Both spectra have the same intensity scale.

- [19] J.E. Carranza, D.W. Hahn, Assessment of the upper particle size limit for quantitative analysis of aerosols using laser induced breakdown spectroscopy, *Anal. Chem.* 74 (2002) 5450–5454.
- [20] V. Hohreiter, D.W. Hahn, Plasma–particle interactions in a laser-induced plasma: implications for laser-induced breakdown spectroscopy, *Anal. Chem.* 78 (2006) 1509–1514.
- [21] E. Vors, L. Salmon, Laser-induced breakdown spectroscopy (LIBS) for carbon single shot analysis of micrometer-sized particles, *Anal. Bioanal. Chem.* 385 (2006) 281–286.
- [22] P.K. Diwakar, P.B. Jackson, D.W. Hahn, Investigation of multi-component aerosol particles and the effect on quantitative laser-induced breakdown spectroscopy: consideration of localized matrix effects, *Spectrochim. Acta Part B* 62 (2007) 1466–1474.
- [23] T. Amodeo, C. Dutouquet, O. Le Bihan, M. Attoui, E. Frejafon, On-line determination of nanometric and sub-micrometric particle physicochemical characteristics using spectral imaging-aided LIBS coupled with a scanning mobility particle sizer, *Spectrochim. Acta Part B* 64 (2009) 1141–1152.
- [24] V. Hohreiter, D.W. Hahn, Calibration effects for laser-induced breakdown spectroscopy of gaseous sample streams: Analyte response of gaseous phase species vs. solid phase species, *Anal. Chem.* 77 (2005) 1118–1124.
- [25] P.S. Dalyander, I.B. Gornushkin, D.W. Hahn, Numerical simulation of laser-induced breakdown spectroscopy: modeling of aerosol analysis with finite diffusion and vaporization effects, *Spectrochim. Acta Part B* 63 (2008) 293–304.
- [26] S. Groh, C.C. Garcia, A. Murtazin, V. Horvatic, K. Niemax, Local effects of atomizing analyte droplets on the plasma parameters of the inductively coupled plasma, *Spectrochim. Acta Part B* 64 (2009) 247–254.
- [27] D.W. Hahn, J.E. Carranza, G.R. Arsenault, H.A. Johnsen, K.R. Hencken, Aerosol generation system for development and calibration of laser-induced breakdown spectroscopy instrumentation, *Rev. Sci. Instrum.* 72 (2001) 3706–3713.
- [28] J.E. Carranza, D.W. Hahn, Sampling statistics and considerations for single-shot analysis using laser induced breakdown spectroscopy, *Spectrochim. Acta Part B* 57 (2002) 779–790.
- [29] B.T. Fisher, H.A. Johnsen, S.G. Buckley, D.W. Hahn, Temporal gating for the optimization of laser-induced breakdown spectroscopy detection and analysis of toxic metals, *Appl. Spectrosc.* 55 (2001) 1312–1319.
- [30] J.E. Carranza, D.W. Hahn, Plasma volume considerations for analysis of gaseous and aerosol samples using laser induced breakdown spectroscopy, *J. Anal. At. Spectrom.* 17 (2002) 1534–1539.
- [31] E.S. Simpson, G.A. Lithgow, S.G. Buckley, Three-dimensional distribution of signal from single monodisperse aerosol particles in a laser induced plasma: initial measurements, *Spectrochim. Acta Part B* 62 (2007) 1460–1465.
- [32] V. Hohreiter, A.J. Ball, D.W. Hahn, Effects of aerosols and laser cavity seeding on spectral and temporal stability of laser-induced plasmas: applications to LIBS, *J. Anal. At. Spectrom.* 19 (2004) 1289–1294.